

Chemistry and Structure of Graphene Oxide via Direct Imaging

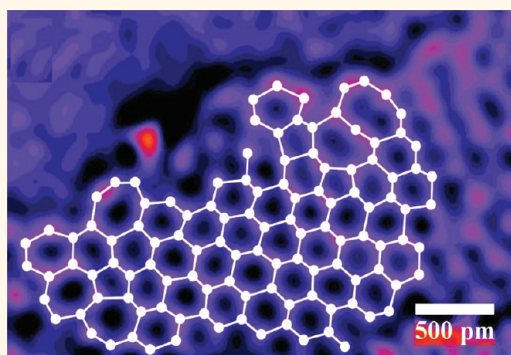
Shreya H. Dave,[†] Chuncheng Gong,[§] Alex W. Robertson,[§] Jamie H. Warner,[§] and Jeffrey C. Grossman^{*,‡}

[†]Department of Mechanical Engineering and [‡]Department of Materials Science & Engineering, Massachusetts Institute of Technology, 77 Massachusetts Avenue, Cambridge, Massachusetts 02139 United States

[§]Department of Materials, University of Oxford, Parks Road, Oxford OX1 3PH, United Kingdom

S Supporting Information

ABSTRACT: Graphene oxide (GO) and reduced GO (rGO) are the only variants of graphene that can be manufactured at the kilogram scale, and yet the widely accepted model for their structure has largely relied on indirect evidence. Notably, existing high-resolution transmission electron microscopy (HRTEM) studies of graphene oxide report long-range order of sp^2 lattice with isolated defect clusters. Here, we present HRTEM evidence of a different structural form of GO, where nanocrystalline regions of sp^2 lattice are surrounded by regions of disorder. The presence of contaminants that adsorb to the surface of the material at room temperature normally prevents direct observation of the intrinsic atomic structure of this defective GO. To overcome this, we use an *in situ* heating holder within an aberration-corrected TEM (AC-TEM) to study the atomic structure of this nanocrystalline graphene oxide from room temperature to 700 °C. As the temperature increases to above 500 °C, the adsorbates detach from the GO and the underlying atomic structure is imaged to be small 2–4 nm crystalline domains within a polycrystalline GO film. By combining spectroscopic evidence with the AC-TEM data, we support the dynamic interpretation of the structural evolution of graphene oxide.



KEYWORDS: graphene oxide, TEM, AC-TEM, surface contaminants

Graphene oxide (GO) is the most readily scalable derivative of graphene, significantly less expensive and considerably more solution-processable when compared to chemical vapor deposition (CVD) graphene and mechanical exfoliation, respectively. GO is formed by heavily oxidizing graphite to chemically exfoliate the flakes of the graphitic stack into mono- and few-layer sheets, depending on the degree of oxidation and postprocessing. Graphite oxide was first prepared by Brodie in 1859,¹ though many commercially implemented methods today rely on modifications to Hummers' method.² The structure of GO is notoriously difficult to characterize and define broadly because of its inherently nonstoichiometric structure and dependence on production parameters. However, according to existing direct imaging evidence, GO is largely considered to have long-range order in sp^2 lattice. Surface contaminants have been characterized as airborne amorphous hydrocarbons,³ oxidative debris,⁴ and patches of disorder as a result of dynamic interactions with its environment^{5,6} and have been observed on both graphene⁷ and GO.^{4,8–11} These contaminants affect the surface properties: increasing the wettability of the graphene⁸ or potentially decreasing the conductivity of graphene oxide.⁴ Further, the surface contaminants pose a challenge to characterizing the intrinsic properties of the material, including

its chemical structure, nature of order and disorder, and defect density, particularly for GO whose structure has been the subject of a number of different, at times conflicting, theories.^{4,8,12–16} In order for graphene or GO to achieve a “killer app”, both these contaminants and the inherent structural transformation of GO must be fully understood.¹⁷

Though direct imaging of the atomic structure of graphene has been achieved extensively using aberration-corrected transmission electron microscopy (AC-TEM), it has proven more challenging to apply similar approaches to GO—particularly more defective GO—due to the increased amounts of surface contaminants relative to graphene that mask the atomic structure. Furthermore, these surface contaminants react with the high energy of the electron beam, leading to structural changes that do not represent the intrinsic GO material and could lead to misinterpreted results. Methods such as baking in air,^{13,18,19} vacuum,^{7,20} or carbon black^{12,21,22} reliably clean graphene for direct observation using microscopy, but our experiments find that none of these methods are

Received: April 8, 2016

Accepted: July 10, 2016

Published: July 10, 2016

effective in cleaning GO or rGO. Recent work has revealed some insights into the atomic structure of relatively defect-free and intact GO by AC-TEM that more strongly resembles graphene in its long-range order.^{3,13,23}

GO is characterized by oxygen functionalization on 20–30% of the basal plane, limiting its electrical and thermal transport and thus its widespread use in electronics and optical applications.^{3,13,18,19,24} Although multiple models for the structure of GO have been proposed (see, for example, refs 20 and 25), the most widely accepted Lerf–Klinowski model reports the decoration of the carbon basal plane with epoxides and hydroxyls, with sheet edges terminated by carboxylic acid functional groups. The oxygen-containing functionalization disrupts the sp^2 order of the graphene backbone such that regions of sp^2 (ordered) are interrupted by the sp^3 (disordered) in the carbon basal plane.¹² Meanwhile, direct observation of GO shows the structure of GO as consisting of long-range-ordered sp^2 regions and characterized by much smaller patches of amorphous material and/or defects, which cannot fully account for the functionalized regions in terms of oxygen atomic fraction.^{3,13,23}

Processing GO to remove oxygen functional groups has been thoroughly explored with chemical,^{19,26} thermal,^{4,8–11,20,22,27} and simulation^{8,28,29} methods. These methods optimize the reduction parameters such that there is sufficient oxygen removal without considerable damage to the graphitic sheet; in other words, removing more oxygen is favorable for conductivity improvements, but lattice vacancies destroy the integrity of the GO flake, limiting its conductivity. Thermogravimetric analysis (TGA) combined with mass spectrometry (MS) shows the removal of CO and CO₂ during thermal annealing and attributes vacancies in the lattice structure to the source of carbon.^{4,12,14,15}

Here, we present a study of the atomic structure of commercially available GO (see Methods), which we will show exhibits short-range order that could be a result of degradation similar to that described by the dynamic structural model (DSM).^{6,30} We characterize the GO with a variety of spectroscopic methods to confirm that the indirect evidence of our samples is consistent with a large range of literature. We also observe a consistent layer of amorphous contaminants that are present in literature examples but not on atomic structural characterization of GO. Though the origin of these surface contaminants is not clear, we believe they could be a combination of byproducts of the oxidation process^{4,9} in addition to airborne hydrocarbons that are more strongly attached to disordered regions in GO. We report on the behavior of the surface contaminants in the vacuum of the TEM and present a method to remove them in order to achieve atomic resolution of the GO structure. Finally, we show that the structure of highly defective GO resembles the Szabó–Dékány model,^{19,25,26} in which the structure of GO consists of nanocrystallines and is disrupted by grain boundaries of disorder.

RESULTS AND DISCUSSION

Surface Contaminants. We conducted a repeatable study of the structure of graphene oxide using aberration-corrected high-resolution TEM at 80 kV. Knock-on damage for pristine graphene is negligible at 80 kV,³¹ and thus graphene and its derivatives are observed at low voltage with spherical aberration (Cs) correction in order to resolve the atomic structure.^{4,12,16,32,33} We prepared samples on heating chips for

TEM (DENS) with a platinum coil shown in Figure 1a. Slits were introduced into the silicon nitride thin film using a

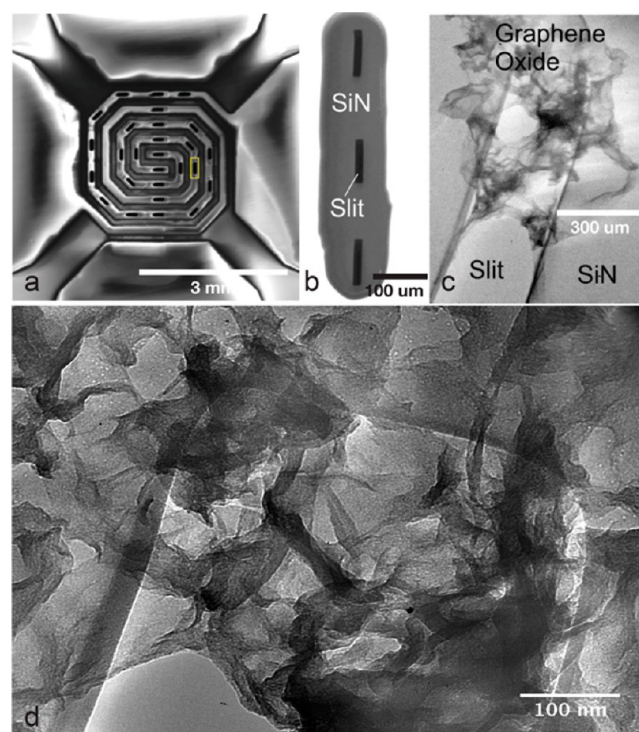


Figure 1. Low-voltage, high-resolution TEM was used to directly observe the structure of graphene oxide. A heating chip containing a platinum coil (a) was used to study the temperature dependence of the structure. A slit was introduced into the thin silicon nitride membrane using a focused ion beam (b) in order to obtain suspended GO. Low-magnification images (c,d) show the macroscopic morphology of graphene oxide: clumped flakes with monolayer regions.

focused ion beam to allow the GO to be suspended across the vacuum for enhanced contrast and atomic resolution imaging, as shown in Figure 1b. Macroscopically, GO is wrinkled and appears clumped consistently through multiple samples, though monolayer regions are visible, as shown in Figure 1c,d.

At room temperature and in the high vacuum of the TEM, direct imaging of the hexagonal lattice structure is inhibited by the presence of amorphous material on the surface of GO, which reacts rapidly under the energy of the beam (see Supplementary Figure 1). This interaction of contamination and the beam is not surprising and was observed in a number of different sample preparation methods, as well as different solvents, graphene oxide feedstocks, and ambient conditions of preparation. It is possible that the relative quantity of amorphous contaminants could be affected by the presence of the electron beam; however, we are not the first to observe such adventitious carbon in the GO system.^{3,13,24,34} Numerous experiments utilizing cleaning methods reported for other two-dimensional materials were conducted and were unable to clear the contamination from GO for imaging,^{7,12,13,18–22} leading us to believe that surface contaminants tend to be more strongly attached to the GO sample than to graphene. At temperatures above 500 °C, the specimen appears more crystalline and we are able to resolve the atomic structure of GO. In Figure 2a, we show a region of graphene oxide in false color to enhance contrast. Both open (monolayer, low contrast) and closed

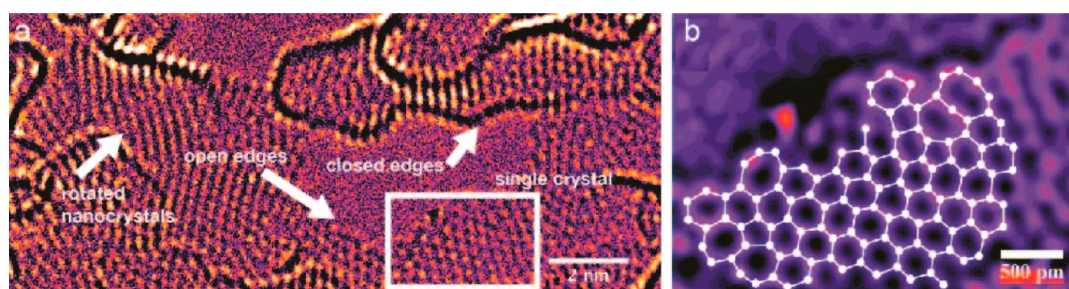


Figure 2. Atomic structure can be resolved using *in situ* heating with AC-TEM at 700 °C with features shown in (a). Sufficient resolution is achieved to identify defects in the bond structure (b). In (b), not all of the atomic structure could be accurately resolved, likely due to structural changes occurring during image acquisition, and only the directly resolved atomic structure is indicated by white dots and lines.

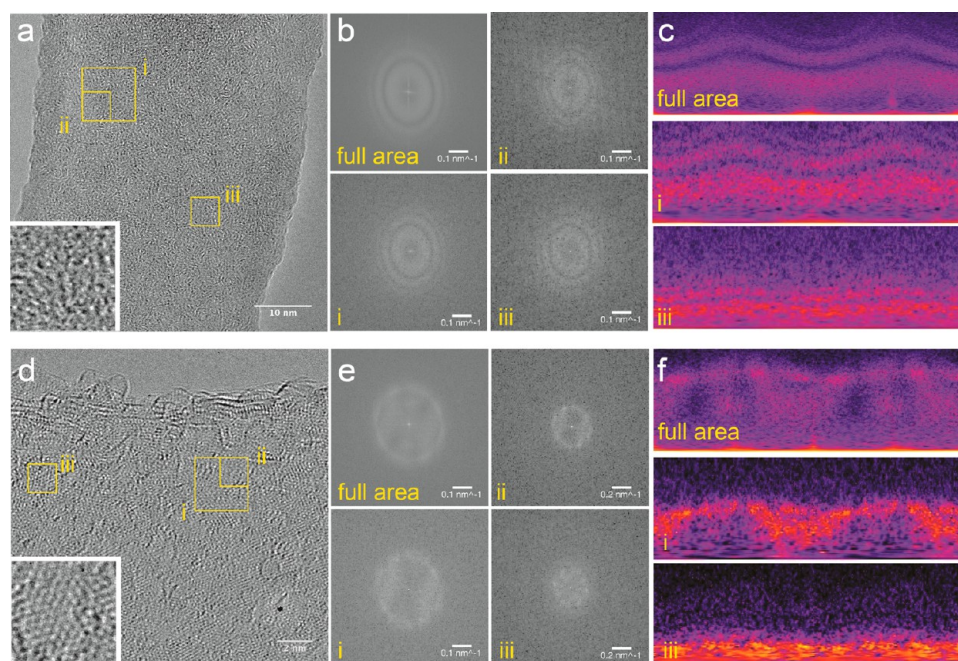


Figure 3. Graphene oxide observed at room temperature (a–c) and 700 °C (d–f) in AC-TEM is notably different in appearance. (a,d) Images of the material at room temperature and 700 °C, respectively, with insets of the 5 nm × 5 nm region iii magnified for each. (b,e) FFTs, both of which have a strong band at $1/d = 1/0.21 \text{ nm}^{-1}$, suggesting polycrystalline graphene domains. (c,f) Polar transforms of the FFTs showing increased order with decreased analysis size. Both the image and the FFTs show high amounts of disorder or amorphous material at room temperature. At 700 °C, although the full region FFT appears similarly amorphous, analysis of smaller components shows the distinct pattern of sp^2 graphene lattice, even in multilayer regions.

(folded over bilayer, high contrast) edges are visible as regions of disorder that separate the nanocrystallites from each other. The high contrast of the closed edges is different from heavier atoms contaminating the sample (Supplementary Figure 2). Figure 2b shows the atomic structure of a region of monolayer GO at a temperature of 700 °C, with sufficient resolution to identify defects (pentagons and heptagons) in the hexagonal sp^2 lattice.

At room temperature, this atomic resolution is not visible. Figure 3 shows the comparison of GO at room temperature (a–c) and at 700 °C (d–f). The fast Fourier transforms (FFTs) for different regions are shown, with the characteristic pattern of sp^2 graphene lattice (spots at $1/d$, where $d = 0.21 \text{ nm}$) observed at 700 °C for small regions. The insets in Figure 3a,d show region iii in each to demonstrate the shift from amorphous contaminants to visible atomic structure.

We believe that the amorphous material is a result of surface contaminants rather than the manifestation of oxygen functionalization of the basal plane for two reasons. First, the

specimen appears more crystalline above 500 °C, which is consistent with previous reports of amorphous hydrocarbon adsorbates on the surface of CVD graphene³⁵ and with the observation of adventitious carbon on GO.^{4,13,23,34} The relative amount of surface contaminants is not defined (as compared to oxide on metals or silicon) but appears to correlate loosely with degree of long-range order as previous HRTEM of GO reports have considerably more visible lattice^{3,13} and ssNMR on lab samples with long-range order do not show large amounts of adsorbed amorphous material.³⁶ Second, the sample again appears amorphous upon cooling to room temperature, suggesting that the contaminants have returned (Figure 4). This has been observed in graphene, but graphene tends to retain areas of visible crystal structure, whereas samples of GO appear qualitatively amorphous throughout.³⁵ In both cases, the surface contaminants return even in the high-vacuum and anti-contamination-protected environment of the TEM, suggesting that their origin is not strictly the oxidation process but instead derived from compounds in the environment, as well.^{4,37}

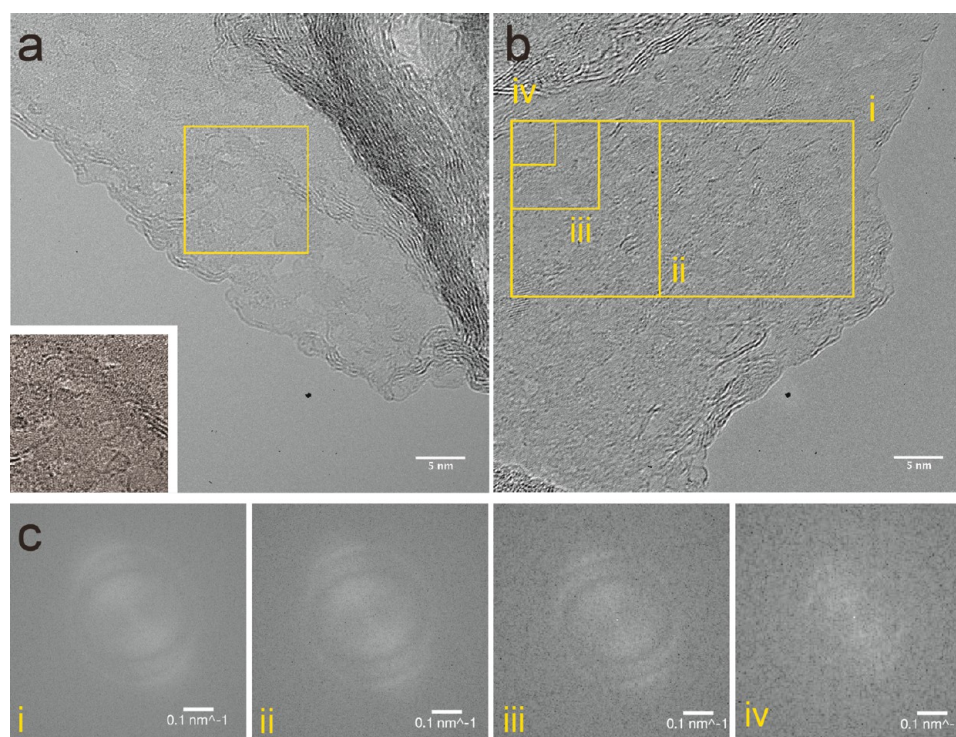


Figure 4. Two different samples show that surface contaminants return to the GO upon cooling from 700 °C to room temperature inside the TEM. Qualitatively, the amount of contaminants appears fewer, but the hexagonal lattice is still not visible. (a) Region with beam damage caused by exposure at room temperature; regions of lighter contrast in the inset are patches of damage that grow with prolonged exposure. The boxed areas in (b) are analyzed with the FFTs in (c).

Figure 4a shows a region imaged at room temperature after first heating to 700 °C. The inset shows the region within the yellow box. The relatively light contrast areas are a result of beam damage and continue to grow with increased beam exposure. Figure 4b shows regions of a cooled sample with their associated FFTs in Figure 4c. These results indicate that any form of spectroscopy conducted at ambient temperature necessarily measures both the contaminants and the intrinsic GO structure. Although it is, as of now, not possible to fully decouple the groups associated with the surface contaminants and the functional groups bonded directly to the basal plane of the GO, we remark on the importance of this observation in any processing, functionalization, or characterization analysis of GO at ambient temperature, even in vacuum.

Nanocrystalline GO. The use of *in situ* heating to image GO provides an opportunity to directly observe the crystal structure of defective GO with atomic resolution. We report on the microstructure of this commercially available GO in order to provide structural information about large-batch, thermally annealed GO and provide a key example to the AC-TEM evidence available to date.

Figure 5 shows graphene oxide imaged at 700 °C. First, we observe that the majority of the drop-cast sample is turbostratically multilayer, with apparent Moiré patterns in the few-layer regions (Figure 5a,b). As expected, the presence of functional groups and surface contaminants appears to decouple interactions between the graphitic lattice of adjacent layers, preventing A–A or A–B–A stacking.^{13,18} Figure 5b has been color-coded to represent the number of layers in each region of the image to assist in distinguishing mono- and multilayer features. Second, we show that the underlying structure of the monolayer regions (Figure 5c,d) is nano-

crystalline, and the sp^2 structure of each crystal is independently rotated with respect to each other. This latter observation is a notable addition in potential structures to the previous reports of amorphous (structural models¹²) and observations of uniform large-area sp^2 (TEM results^{3,13,24}) and is characterized quantitatively through FFTs of regions in the image. The line scans in Figure 5e show increasing sharpness of the polar FFT, demonstrating increasing order for smaller regions.

The average size of the sp^2 nanocrystallites was calculated using around 10 images collected at 700 °C. The boundaries between crystallites are apparent in single-layer areas but are less visible in regions where the material is few-layer or multilayer. The intra- and interlayer rotation between crystallites results in a film that appears amorphous in FFTs of regions larger than ~ 100 nm², even in thin regions. When an FFT is taken of a much smaller region, one to a few crystallites are clear, with the average size of a single crystal of ~ 2 nm². We note that the size of the crystalline regions does not change with time at the elevated temperature and under the exposure of the beam in order to rule out heat-induced domain size changes. Since mechanically exfoliated graphene from graphitic parent material has larger grain sizes, the disorder is likely introduced during the oxidation or washing process, suggesting that tunable transport in rGO derived from chemical exfoliation will remain limited without sufficient temperature for sp^2 recrystallization (>1000 °C).

Evolution of Annealed GO. In order to decouple the oxygen removal from the surface contaminants, we compare these HRTEM results with spectroscopic data. Unlike graphene, GO undergoes chemical changes upon heating, including carbon removal from the lattice site.³⁸ In addition to the removal of amorphous surface contaminants, oxygen-

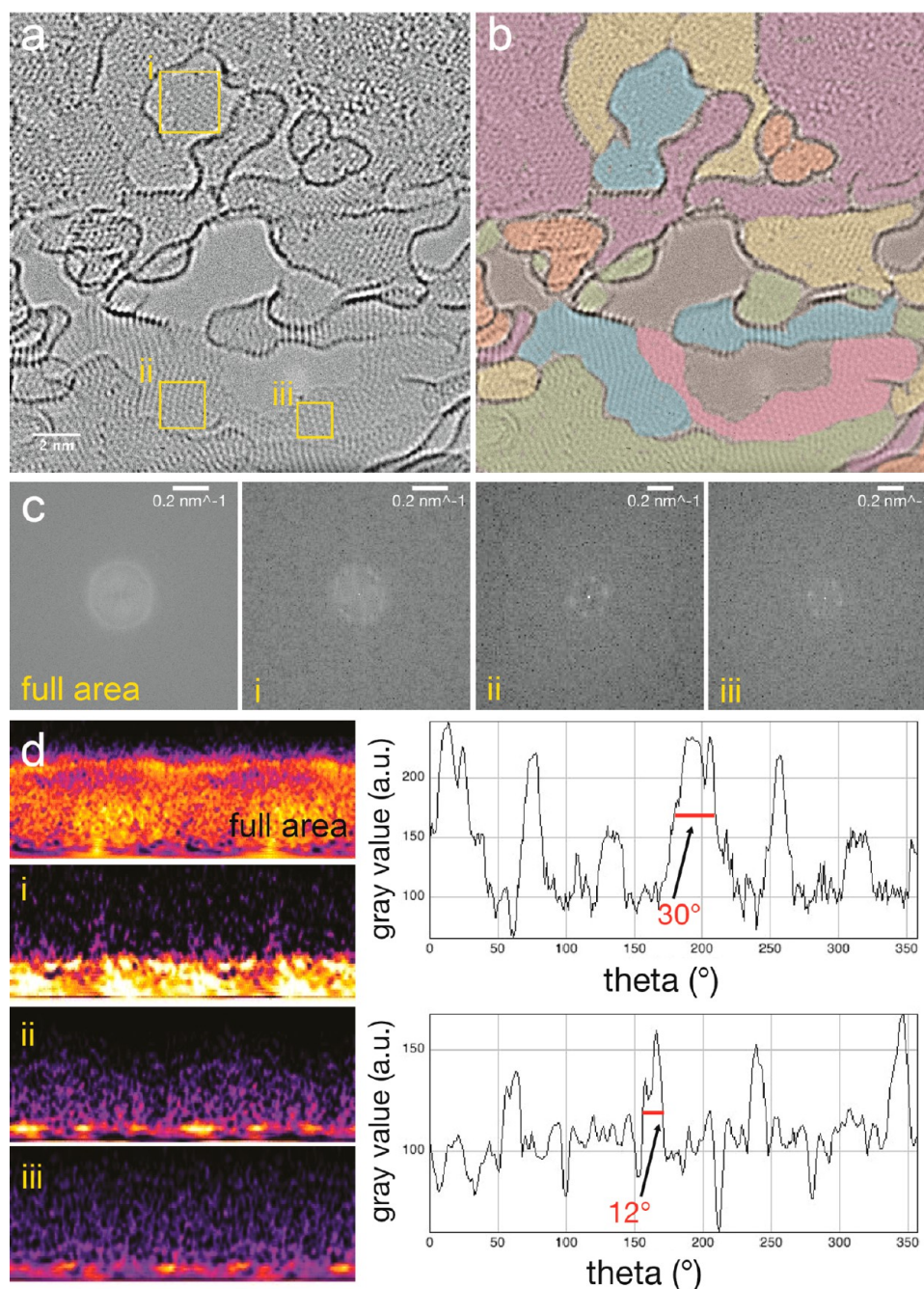


Figure 5. (a) High-resolution image of mono- and few-layer graphene oxide at 700 °C imaged with an *in situ* TEM heating holder. (b) Overlaid color represents layers of the material, showing turbostratic stacking and thicker and thinner regions. (c) False-color polar transforms of the FFTs (θ x -axis, $1/d$ y -axis). (d) Regions of the image show an increase in sharpness of the band and points at $1/d$ spacing of $1/0.19$ to $1/0.21$ nm^{-1} . (e) Line scans show the increase in sharpness of the lattice points from regions ii and iii.

containing functional groups attached to the basal plane are removed with increasing temperature, as is reported by many others.^{22,28,39} Further, simulations show that thermal annealing in the absence of surface contaminants reduces the oxygen content of rGO.^{28,29} However, here, despite a reduction in oxygen content of 70% when heated to 700 °C in a vacuum, cooled, and then analyzed, the correlating images consistently show amorphous material.

To determine whether heating to 700 °C dramatically changes the nanocrystalline nature of GO, we collected selected area diffraction patterns (SADP) of GO that had not been heated previously with decreasing selected area aperture sizes.

We deposited GO on lacey carbon grids and examined the diffraction patterns from GO flakes that were very thin and appeared monolayer and flat in their projection with respect to the electron beam. Figure 6a shows a flake of graphene oxide with SADPs for small area (200 nm in Figure 6b) and the yellow region indicated (Figure 6c) and their associated line traces. Though much more order is detected in the smaller region in b, the area is still demonstrably polycrystalline. Figure 6d shows the SADP for monolayer graphene grown by CVD on Cu using CH_4 according to prior reported methods and transferred to a TEM grid for comparison.⁴⁰ Though it is possible that the GO undergoes structural transformation

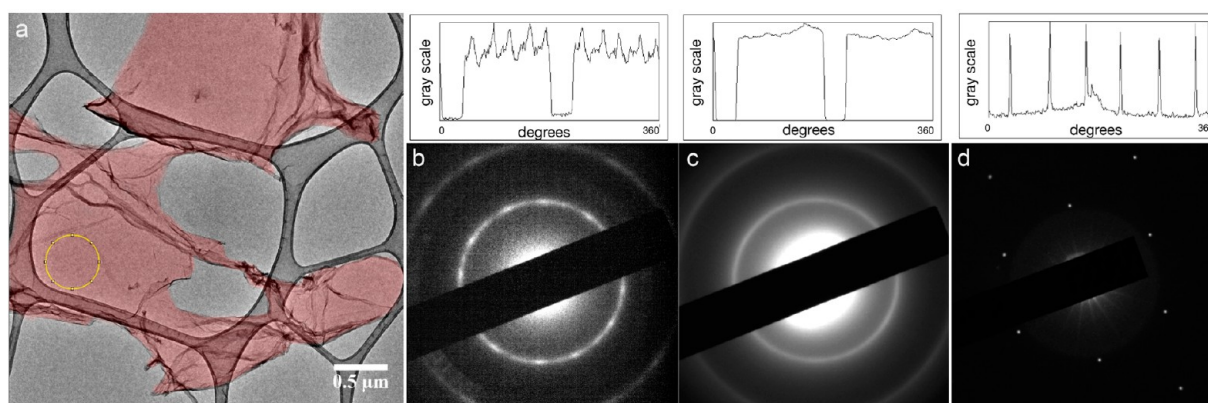


Figure 6. (a) A graphene oxide flake suspended on a lacey carbon grid (b) SADP with polycrystallinity in a region of about 200 nm, and (c) SADP for the region inside the yellow circle. (d) Sharp spots for crystalline SADP for monolayer graphene. Line scans for each demonstrate the range in order that is observed.

during the heating process, we provide these data as one piece of evidence suggesting that the polycrystallinity exists prior to annealing, but that the surface contaminants inhibit their direct observation.

Annealing to 700 °C most notably, and unsurprisingly, reduces the oxygen content of the GO (Supplementary Figure 3). Meanwhile, heating does not change the shape or position of the characteristic D (1330 cm^{-1}) and G (1590 cm^{-1}) Raman peak shapes drastically (Supplementary Figure 4). Similarly, the I_D/I_G ratio changes only slightly from 1.09 to 1.13 (just outside standard error bars) and suggests little change to the crystallite size and that high-temperature images are representative of the unheated GO, though defects could be introduced into the lattice upon heating. Moreover, the AC-TEM results very well support the models presented for the Raman spectroscopy of graphene and graphene oxide presented recently.^{41–43}

Finally, Fourier transform infrared spectroscopy attenuated total reflectance (FTIR-ATR) (Supplementary Figure 5) shows qualitatively that the same functional groups are present after annealing as before. However, as with prior TGA studies under nitrogen, we observe dehydration of adsorbed water around 100 °C (Supplementary Figure 6). Also consistent with prior studies, we observe a slight change in slope near 400 °C, which we would instead attribute to the release of amorphous surface contaminants rather than oxygen-containing functional groups and carbon from the sp^2 lattice. Further, direct observation of *in situ* heating shows no significant carbon removal from the lattice even upon extended periods of heating up to 700 °C, which demonstrates its stability at such a high temperature.

CONCLUSIONS

These results show how using an *in situ* heating holder can help elucidate the atomic structure of GO as a function of temperature by removing surface-adsorbed material that inhibits AC-TEM imaging. Our evidence supports alternative models to the structure of GO, for example, the DSM described by Dimiev *et al.*, and is importantly a TEM study of bulk-produced GO with short-range order. In order to relate the structure of the GO directly with models such as the DSM, a progressive experiment utilizing *in situ* heating and water or strong base exposure of the time scale of months could be conducted. The nanocrystalline nature of GO has implications in the efforts of restoration of efficient transport for electronic applications. The ubiquitous presence of amorphous contam-

inants on defective GO at room temperature has implications for GO design as a catalyst substrate, enhancing electrical conductivity, or the stable cross-linking of GO sheets for membrane separation processes, revising our interpretation of carbon and oxygen removal, lattice defects, and spectroscopic data. With *in situ* heating for TEM, the evolution of the graphene oxide structure is revealed beyond long-range order. The rapid degradation of the GO sample under electron beam irradiation at 80 kV at room temperature shows that care must be taken when analyzing GO samples by TEM, and detecting defects or nanopores that are intrinsic to the material is extremely challenging.

METHODS

Nanoplatelet graphene oxide (>99% single layer, average flake size 90 nm) was purchased from Graphene Supermarket to represent GO produced at scale and was used for all measurements reported herein. GO was produced using a modified Hummers' method, and samples were washed in water for purification. No processing method above 80 °C was used in order to maintain the stability of the GO framework. Low-magnification TEM shows that the majority of the GO flakes after dispersion in isopropyl alcohol (IPA) were actually larger (Supplementary Figure 6) but could be due to the size of holes in the grid, with small flakes falling through the support material. Annealing was conducted in a furnace under vacuum (<30 mTorr) to mimic TEM conditions. The heating rate in the CVD was about 1 °C per second. Samples were annealed for 1 h to allow them to achieve a steady state, although most chemical changes (oxygen removal) occur within seconds to minutes of reaching temperature. Samples were then evaluated using Raman spectroscopy, X-ray photoelectron spectroscopy (XPS), TGA, and FTIR-ATR in addition to TEM to monitor evolution during heating. All spectroscopic data collection was conducted at room temperature and ambient pressure except the XPS, which was collected under vacuum.

Sample Preparation. GO samples were purchased from Graphene Supermarket (nanographene oxide) to replicate bulk processing conditions of a modified Hummers' method. GO was dispersed in IPA and drop-cast onto silicon nitride chips for spectroscopic analysis and DENS heating chips for TEM imaging. The heating chips were prepared by introducing a slit in the silicon nitride membrane using a focused ion beam for free-standing graphene. Annealed samples were thermally treated in a custom-built CVD chamber at a pressure of ~5–30 mTorr (vacuum) and with the ends of the tube open to the ambient environment (air) for 30 min to 1 h.

Transmission Electron Microscopy. HRTEM images were collected using a JEOL MCO 2200 aberration-corrected transmission electron microscope operated at an accelerating voltage of 80 kV. Data

were recorded using a Gatan Ultrascan 4K × 4K CCD camera with 1–2 s acquisition times and 2 pixel binning.

SADPs were collected using a JEOL 2100 HRTEM operated at an accelerating voltage of 200 kV. Using a higher voltage for SADPs does not damage the GO sample due to lower beam intensity.¹⁶

Image Processing. Processing of TEM images was conducted using ImageJ. Band-pass filters (1–100 pixels) were used to remove uneven illumination on all presented images. No image reconstruction was used. Line profiles and false-color images were generated using a polar transformer plugin for ImageJ to process FFTs. False-color images are LUT Fire in ImageJ.

In Situ Heating Holder. We used a commercially available *in situ* heating holder from DENS Solutions (SH30-4M-FS). Heating the sample was achieved by passing a current through a platinum resistive coil imbedded in the TEM chip (DENS Solutions DENS-C-30). The resistance of the platinum coil was monitored in a four-point configuration, and the temperature was calculated using the Callendar–Van Dusen equation (with calibration constants provided by the manufacturer). Slits were introduced into the silicon nitride film of the TEM chips using a Zeiss NVision focused ion beam.

Raman Spectroscopy. Micro-Raman spectra were collected using a Horiba LabRAM 800 HR spectrometer equipped with He–Ne (632.817) laser and no filter. Samples were tested for degradation under the intensity of the laser, and no degradation was found. Collection time was 5 s, an average of 5–10 times; spot size was ~800 nm in diameter, had a power of <1 mW at the sample surface, and was corrected for fluorescence. Data were collected across the thin film on 6–1 points and averaged to observe film uniformity and reduce error bars. All graphs include standard error bars. Data were analyzed using LabSpec, and peak intensity (area) was used for the calculation of the I_D/I_G ratio.

X-ray Photoelectron Spectroscopy. XPS data were collected using a Thermo Fisher Scientific K-Alpha with Al K α radiation. In order to reduce surface charging, XPS data were collected with the flood gun, which consists of low-energy electrons and ions that neutralize the surface of the GO. The XPS samples were prepared with a dilute solution of GO (in IPA) drop-cast onto silicon nitride. The use of silicon nitride is to eliminate any contribution of oxidation of the substrate to the peaks. The samples were taken with a 400 μ m spot size on regions that appear visually homogeneous. Finally, the survey spectra detected the substrate, which indicates that the film is thin, further helping to suppress charging. Data were analyzed using CasaXPS survey spectra to calculate oxygen concentration.

FTIR-ATR Spectroscopy. Fourier transform infrared spectroscopy was conducted using a germanium attenuated total reflectance crystal in a Thermo Fisher FTIR6700 at ambient conditions. Background and sample scans were taken at a sample rate of 64.

Thermogravimetric Analysis. TGA data were collected using TA Instruments Q500 in air and nitrogen as an inert environment with about 70 mg of GO. The heating rate was 10 °C/min. Data were analyzed using Universal Analysis 2000.

ASSOCIATED CONTENT

Supporting Information

The Supporting Information is available free of charge on the ACS Publications website at DOI: 10.1021/acs.nano.6b02391.

Additional information and figures (PDF)

AUTHOR INFORMATION

Corresponding Author

*E-mail: jcg@mit.edu.

Author Contributions

S.H.D. and J.C.G. conceived the idea. S.H.D. and J.H.W. designed the experiments, which were implemented and carried out by S.H.D., C.G., and A.W.R. The data were analyzed and the manuscript was written from contributions by S.H.D., J.H.W., and J.C.G.

Notes

The authors declare no competing financial interest.

ACKNOWLEDGMENTS

We thank Dr. Nicola Ferralis for the assistance in interpretation of Raman spectroscopy, and Abdullah Y. Alsalloum for assistance in acquisition of some Raman spectroscopic data. We also thank Adam Graham of CNS for help with imaging methods. We greatly appreciate funding and support for this research from the Deshpande Center for Technological Innovation at MIT. This work made use of the Center for Nanoscale Systems (CNS), a member of the National Nanotechnology Infrastructure Network (NINN), which is supported by the National Science Foundation under NSF Award No. ECS-0335765. CNS is part of Harvard University. J.H.W. thanks the Royal Society for support.

REFERENCES

- (1) Brodie, B. C. On the Atomic Weight of Graphite. *Philos. Trans. R. Soc. London* **1859**, *149*, 249–259.
- (2) Hummers, W. S.; Offeman, R. E. Preparation of Graphitic Oxide. *J. Am. Chem. Soc.* **1958**, *80*, 1339–1339.
- (3) Gómez-Navarro, C.; Meyer, J. C.; Sundaram, R. S.; Chuvilin, A.; Kurasch, S.; Burghard, M.; Kern, K.; Kaiser, U. Atomic Structure of Reduced Graphene Oxide. *Nano Lett.* **2010**, *10*, 1144–1148.
- (4) Rourke, J. P.; Pandey, P. A.; Moore, J. J.; Bates, M.; Kinloch, I. A.; Young, R. J.; Wilson, N. R. The Real Graphene Oxide Revealed: Stripping the Oxidative Debris From the Graphene-Like Sheets. *Angew. Chem., Int. Ed.* **2011**, *50*, 3173–3177.
- (5) Dimiev, A. M.; Alemany, L. B.; Tour, J. M. Graphene Oxide. Origin of Acidity, Its Instability in Water, and a New Dynamic Structural Model. *ACS Nano* **2013**, *7*, 576–588.
- (6) Dimiev, A. M.; Polson, T. A. Contesting the Two-Component Structural Model of Graphene Oxide and Reexamining the Chemistry of Graphene Oxide in Basic Media. *Carbon* **2015**, *93*, 544–554.
- (7) Robertson, A. W.; Ford, C.; He, K.; Kirkland, A. I.; Watt, A. A. R.; Warner, J. H. PbTe Nanocrystal Arrays on Graphene and the Structural Influence of Capping Ligands. *Chem. Mater.* **2014**, *26*, 1567–1575.
- (8) Li, Z.; Wang, Y.; Kozbial, A.; Shenoy, G.; Zhou, F.; McGinley, R.; Ireland, P.; Morganstein, B.; Kunkel, A.; Surwade, S. P.; Li, L.; Liu, H. Effect of Airborne Contaminants on the Wettability of Supported Graphene and Graphite. *Nat. Mater.* **2013**, *12*, 925–931.
- (9) Bonanni, A.; Ambrosi, A.; Chua, C. K.; Pumbera, M. Oxidation Debris in Graphene Oxide Is Reponsible for Its Inherent Electroactivity. *ACS Nano* **2014**, *8*, 4197–4204.
- (10) Li, Z.; Kozbial, A.; Nioradze, N.; Parobek, D.; Shenoy, G. J.; Salim, M.; Amemiya, S.; Li, L.; Liu, H. Water Protects Graphitic Surface From Airborne Hydrocarbon Contamination. *ACS Nano* **2016**, *10*, 349–359.
- (11) Li, X.; Yang, X.; Jia, L.; Ma, X.; Zhu, L. Carbonaceous Debris That Resided in Graphene Oxide/Reduced Graphene Oxide Profoundly Affect Their Electrochemical Behaviors. *Electrochem. Commun.* **2012**, *23*, 94–97.
- (12) Lerf, A.; He, H.; Forster, M.; Klinowski, J. Structure of Graphite Oxide Revisited. *J. Phys. Chem. B* **1998**, *102*, 4477–4482.
- (13) Erickson, K.; Erni, R.; Lee, Z.; Alem, N.; Gannett, W.; Zettl, A. Determination of the Local Chemical Structure of Graphene Oxide and Reduced Graphene Oxide. *Adv. Mater.* **2010**, *22*, 4467–4472.
- (14) Larciprete, R.; Fabris, S.; Sun, T.; Lacovig, P.; Baraldi, A.; Lizzit, S. Dual Path Mechanism in the Thermal Reduction of Graphene Oxide. *J. Am. Chem. Soc.* **2011**, *133*, 17315–17321.
- (15) Eigler, S.; Dotzer, C.; Hirsch, A.; Enzelberger, M.; Müller, P. Formation and Decomposition of CO₂ Intercalated Graphene Oxide. *Chem. Mater.* **2012**, *24*, 1276–1282.
- (16) Wilson, N. R.; Pandey, P. A.; Beanland, R.; Young, R. J.; Kinloch, I. A.; Gong, L.; Liu, Z.; Suenaga, K.; Rourke, J. P.; York, S. J.

- Sloan, J. Graphene Oxide: Structural Analysis and Application as a Highly Transparent Support for Electron Microscopy. *ACS Nano* **2009**, *3*, 2547–2556.
- (17) Peplow, M. Graphene Booms in Factories but Lacks a Killer App. *Nature* **2015**, *522*, 268–269.
- (18) Eda, G.; Chhowalla, M. Chemically Derived Graphene Oxide: Towards Large-Area Thin-Film Electronics and Optoelectronics. *Adv. Mater.* **2010**, *22*, 2392–2415.
- (19) Loh, K. P.; Bao, Q.; Eda, G.; Chhowalla, M. Graphene Oxide as a Chemically Tunable Platform for Optical Applications. *Nat. Chem.* **2010**, *2*, 1015–1024.
- (20) Dreyer, D. R.; Park, S.; Bielawski, C. W.; Ruoff, R. S. The Chemistry of Graphene Oxide. *Chem. Soc. Rev.* **2009**, *39*, 228.
- (21) Algara-Siller, G.; Lehtinen, O.; Turchanin, A.; Kaiser, U. Dry-Cleaning of Graphene. *Appl. Phys. Lett.* **2014**, *104*, 153115.
- (22) Mattevi, C.; Eda, G.; Agnoli, S.; Miller, S.; Mkhoyan, K. A.; Celik, O.; Mastrogianni, D.; Granozzi, G.; Garfunkel, E.; Chhowalla, M. Evolution of Electrical, Chemical, and Structural Properties of Transparent and Conducting Chemically Derived Graphene Thin Films. *Adv. Funct. Mater.* **2009**, *19*, 2577–2583.
- (23) Pantelic, R. S.; Meyer, J. C.; Kaiser, U.; Baumeister, W.; Plitzko, J. M. Graphene Oxide: a Substrate for Optimizing Preparations of Frozen-Hydrated Samples. *J. Struct. Biol.* **2010**, *170*, 152–156.
- (24) Pantelic, R. S.; Meyer, J. C.; Kaiser, U.; Baumeister, W.; Plitzko, J. M. Graphene Oxide: a Substrate for Optimizing Preparations of Frozen-Hydrated Samples. *J. Struct. Biol.* **2010**, *170*, 152–156.
- (25) Szabó, T.; Berkesi, O.; forgo, P.; jospovits, K.; sanakis, Y.; petridis, D.; Dékány, I. Evolution of Surface Functional Groups in a Series of Progressively Oxidized Graphite Oxides. *Chem. Mater.* **2006**, *18*, 2740–2749.
- (26) Feng, H.; Cheng, R.; Zhao, X.; Duan, X.; Li, J. A Low-Temperature Method to Produce Highly Reduced Graphene Oxide. *Nat. Commun.* **2013**, *4*, 1539–7.
- (27) Eda, G.; Fanchini, G.; Chhowalla, M. Large-Area Ultrathin Films of Reduced Graphene Oxide as a Transparent and Flexible Electronic Material. *Nat. Nanotechnol.* **2008**, *3*, 270–274.
- (28) Bagri, A.; Mattevi, C.; Acik, M.; Chabal, Y. J.; Chhowalla, M.; Shenoy, V. B. Structural Evolution During the Reduction of Chemically Derived Graphene Oxide. *Nat. Chem.* **2010**, *2*, 581–587.
- (29) Lin, L.-C.; Grossman, J. C. Atomistic Understandings of Reduced Graphene Oxide as an Ultrathin-Film Nanoporous Membrane for Separations. *Nat. Commun.* **2015**, *6*, 8335.
- (30) Dimiev, A. M.; Alemany, L. B.; Tour, J. M. Graphene Oxide. Origin of Acidity, Its Instability in Water, and a New Dynamic Structural Model. *ACS Nano* **2013**, *7*, 576–588.
- (31) Girit, C.; Meyer, J.; Erni, R.; Rossell, M. D.; Kisielowski, C.; Yang, L.; Park, C.-H.; Crommie, M. F.; Cohen, M.; Louie, S.; Zettl, A. Graphene at the Edge: Stability and Dynamics. *Science* **2009**, *323*, 1705–1708.
- (32) Warner, J. H.; Margine, E. R.; Mukai, M.; Robertson, A. W.; Giustino, F.; Kirkland, A. I. Dislocation-Driven Deformations in Graphene. *Science* **2012**, *337*, 209–212.
- (33) Bell, D. C.; Russo, C. J.; Benner, G. Sub-Ångstrom Low-Voltage Performance of a Monochromated, Aberration-Corrected Transmission Electron Microscope. *Microsc. Microanal.* **2010**, *16*, 386–392.
- (34) Mkhoyan, K. A.; Contryman, A. W.; Silcox, J.; Stewart, D. A.; Eda, G.; Mattevi, C.; Miller, S.; Chhowalla, M. Atomic and Electronic Structure of Graphene-Oxide. *Nano Lett.* **2009**, *9*, 1058–1063.
- (35) He, K.; Robertson, A. W.; Gong, C.; Allen, C. S.; Xu, Q.; Zandbergen, H.; Grossman, J. C.; Kirkland, A. I.; Warner, J. H. Controlled Formation of Closed-Edge Nanopores in Graphene. *Nanoscale* **2015**, *7*, 11602.
- (36) Casabianca, L. B.; Shaibat, M. A.; Cai, W. W.; Park, S.; Piner, R.; Ruoff, R. S.; Ishii, Y. NMR-Based Structural Modeling of Graphite Oxide Using Multidimensional ^{13}C Solid-State NMR and *Ab Initio* Chemical Shift Calculations. *J. Am. Chem. Soc.* **2010**, *132*, 5672–5676.
- (37) Thomas, H. R.; Day, S. P.; Woodruff, W. E.; Vallés, C.; Young, R. J.; Kinloch, I. A.; Morley, G. W.; Hanna, J. V.; Wilson, N. R.; Rourke, J. P. Deoxygenation of Graphene Oxide: Reduction or Cleaning? *Chem. Mater.* **2013**, *25*, 3580–3588.
- (38) Eigler, S.; Grimm, S.; Hirsch, A. Investigation of the Thermal Stability of the Carbon Framework of Graphene Oxide. *Chem. - Eur. J.* **2014**, *20*, 984–989.
- (39) Chen, C.-M.; Zhang, Q.; Yang, M.-G.; Huang, C.-H.; Yang, Y.-G.; Wang, M.-Z. Structural Evolution During Annealing of Thermally Reduced Graphene Nanosheets for Application in Supercapacitors. *Carbon* **2012**, *50*, 3572–3584.
- (40) Wu, Y. A.; Fan, Y.; Speller, S.; Creeth, G. L.; Sadowski, J. T.; He, K.; Robertson, A. W.; Allen, C. S.; Warner, J. H. Large Single Crystals of Graphene on Melted Copper Using Chemical Vapor Deposition. *ACS Nano* **2012**, *6*, 5010–5017.
- (41) Cançado, L. G.; Jorio, A.; Ferreira, E. H. M.; Stavale, F.; Achete, C. A.; Capaz, R. B.; Moutinho, M. V. O.; Lombardo, A.; Kulmala, T. S.; Ferrari, A. C. Quantifying Defects in Graphene via Raman Spectroscopy at Different Excitation Energies. *Nano Lett.* **2011**, *11*, 3190–3196.
- (42) Lucchese, M. M.; Stavale, F.; Ferreira, E. H. M.; Vilani, C.; Moutinho, M. V. O.; Capaz, R. B.; Achete, C. A.; Jorio, A. Quantifying Ion-Induced Defects and Raman Relaxation Length in Graphene. *Carbon* **2010**, *48*, 1592–1597.
- (43) Eigler, S.; Hof, F.; Enzelberger-Heim, M.; Grimm, S.; Müller, P.; Hirsch, A. Statistical Raman Microscopy and Atomic Force Microscopy on Heterogeneous Graphene Obtained After Reduction of Graphene Oxide. *J. Phys. Chem. C* **2014**, *118*, 7698–7704.